The Detection of a Population of Submillimeter-Bright, Strongly Lensed Galaxies

Mattia Negrello, *et al.*

Science **330**, 800 (2010);
DOI: 10.1126/science.1193420

The Detection of a Population of Submillimeter-Bright, Strongly Lensed Galaxies

Mattia Negrello,[1*] R. Hopwood,[1] G. De Zotti,[2,3] A. Cooray,[4] A. Verma,[5] J. Bock,[6,7] D. T. Frayer,[8] M. A. Gurwell,[9] A. Omont,[10] R. Neri,[11] H. Dannerbauer,[12] L. L. Leeuw,[13,14] E. Barton,[4] J. Cooke,[4,7] S. Kim,[4] E. da Cunha,[15] G. Rodighiero,[16] P. Cox,[11] D. G. Bonfield,[17] M. J. Jarvis,[17] S. Serjeant,[1] R. J. Ivison,[18,19] S. Dye,[20] I. Aretxaga,[21] D. H. Hughes,[21] E. Ibar,[18] F. Bertoldi,[22] I. Valtchanov,[23] S. Eales,[20] L. Dunne,[24] S. P. Driver,[25] R. Auld,[20] S. Buttiglione,[2] A. Cava,[26,27] C. A. Grady,[28,29] D. L. Clements,[30] A. Dariush,[20] J. Fritz,[31] D. Hill,[25] J. B. Hornbeck,[32] L. Kelvin,[25] G. Lagache,[33,34] M. Lopez-Caniego,[35] J. Gonzalez-Nuevo,[3] S. Maddox,[24] E. Pascale,[20] M. Pohlen,[20] E. E. Rigby,[24] A. Robotham,[25] C. Simpson,[36] D. J. B. Smith,[24] P. Temi,[37] M. A. Thompson,[17] B. E. Woodgate,[38] D. G. York,[39] J. E. Aguirre,[40] A. Beelen,[34] A. Blain,[7] A. J. Baker,[41] M. Birkinshaw,[42] R. Blundell,[9] C. M. Bradford,[6,7] D. Burgarella,[43] L. Danese,[3] J. S. Dunlop,[18] S. Fleuren,[44] J. Glenn,[45] A. I. Harris,[46] J. Kamenetzky,[45] R. E. Lupu,[40] R. J. Maddalena,[8] B. F. Madore,[47] P. R. Maloney,[45] H. Matsuhara,[48] M. J. Michaowski,[19] E. J. Murphy,[49] B. J. Naylor,[6] H. Nguyen,[6] C. Popescu,[50] S. Rawlings,[5] D. Rigopoulou,[5,51] D. Scott,[52] K. S. Scott,[40] M. Seibert,[47] I. Smail,[53] R. J. Tuffs,[54] J. D. Vieira,[7] P. P. van der Werf,[19,55] J. Zmuidzinas[6,7]

Gravitational lensing is a powerful astrophysical and cosmological probe and is particularly valuable at submillimeter wavelengths for the study of the statistical and individual properties of dusty star-forming galaxies. However, the identification of gravitational lenses is often time-intensive, involving the sifting of large volumes of imaging or spectroscopic data to find few candidates. We used early data from the Herschel Astrophysical Terahertz Large Area Survey to demonstrate that wide-area submillimeter surveys can simply and easily detect strong gravitational lensing events, with close to 100% efficiency.

When the light from a distant galaxy is deflected by a foreground mass—commonly a massive elliptical galaxy or galaxy cluster or group—its angular size and brightness are increased, and multiple images of the same source may form. This phenomenon is commonly known as gravitational lensing (*1*) and can be exploited in the study of high-redshift galaxy structures down to scales difficult (if not impossible) to probe with the largest telescopes at present (*2–4*) and to detect intrinsically faint objects. Surveys conducted at submillimeter wavelengths can particularly benefit from gravitational lensing because submillimeter telescopes have limited spatial resolution and consequently high source confusion, which makes it difficult to directly probe the populations responsible for the bulk of background submillimeter emission (*5*, *6*). In addition, galaxies detected in blank-field submillimeter surveys generally suffer severe dust obscuration and are therefore challenging to detect and study at optical and near-infrared (NIR) wavelengths. By alleviating the photon starvation, gravitational lensing facilitates follow-up observations of galaxies obscured by dust and in particular the determination of their redshift (*7*). Previous submillimeter searches for highly magnified background galaxies have predominantly targeted galaxy cluster fields (*8*). In fact, a blind search for submillimeter lensing events requires a large area because of their rarity and sub-arcseconds angular resolutions to reveal multiple images of the same background galaxies.

Although the first requirement has recently been fulfilled, thanks to the advent of the South Pole Telescope (SPT) (*9*) and the Herschel Space Observatory (Herschel) (*10*), the second is still the prerogative of ground-based interferometric facilities, such as the Submillimeter Array (SMA) and the IRAM Plateau de Bure Interferometer (PdBI), which because of their small instantaneous field of view are aimed at follow-up observations rather than large-area survey campaigns. Nevertheless, several authors (*11–14*) have suggested that a simple selection in flux density, rather than surveys for multiply imaged sources, can be used to easily and efficiently select samples of strongly gravitationally lensed galaxies in wide-area submillimeter and millimeter surveys. The explanation for this lies in the steepness of

[1]Department of Physics and Astronomy, The Open University, Walton Hall, Milton Keynes, MK7 6AA, UK. [2]Istituto Nazionale di Astrofisica, Osservatorio Astronomico di Padova, Vicolo Osservatorio 5, I-35122 Padova, Italy. [3]Scuola Internazionale Superiore di Studi Avanzati, Via Bonomea 265, I-34136 Trieste, Italy. [4]Department of Physics and Astronomy, University of California, Irvine, CA 92697, USA. [5]Oxford Astrophysics, Denys Wilkinson Building, University of Oxford, Keble Road, Oxford OX1 3RH, UK. [6]Jet Propulsion Laboratory (JPL), Pasadena, CA 91009, USA. [7]California Institute of Technology, Pasadena, CA 91125, USA. [8]National Radio Astronomy Observatory, Post Office Box 2, Green Bank, WV 24944, USA. [9]Harvard-Smithsonian Center for Astrophysics, Cambridge, MA 02138, USA. [10]Institut d'Astrophysique de Paris, Universitte Pierre et Marie Curie and CNRS, 98 bis boulevard Arago, 75014 Paris, France. [11]Institut de Radioastronomie Millimétrique (IRAM), 300 rue de la piscine, 38406 Saint-Martin d'Hères, France. [12]Laboratoire Astrophysique, Instrumentation et Modélisation Paris Sarclay, Commissariat à l'Énergie Atomique (CEA)/Direction des Sciences de la Matière–CNRS–Université Paris Diderot, Institut de Recherche sur les lois fondamentales d l'Universe/Service d'Astrophysique, CEA Saclay, Orme des Merisiers, F-91191 Gif-sur-Yvette Cedex, France. [13]Physics Department, University of Johannesburg, Post Office Box 524, Auckland Park 2006, South Africa. [14]SETI Institute, 515 North Whisman Avenue, Mountain View, CA 94043, USA. [15]Department of Physics, University of Crete, 71003 Heraklion, Greece. [16]Dipartimento di Astronomia, Universitá di Padova, Vicolo Osservatorio 2, I-35122 Padova, Italy. [17]Centre for Astrophysics Research, Science and Technology Research Institute, University of Hertfordshire, Herts AL10 9AB, UK. [18]UK Astronomy Technology Center, Royal Observatory Edinburgh, Edinburgh EH9 3HJ, UK. [19]Scottish Universities Physics Alliance, Institute for Astronomy, University of Edinburgh, Royal Observatory, Edinburgh EH9 3HJ, UK. [20]School of Physics and Astronomy, Cardiff University, The Parade, Cardiff CF24 3AA, UK. [21]Instituto Nacional de Astrofísica, Óptica y Electrónica, Apartado Postal 51 y 216, 72000 Puebla, Mexico. [22]Argelander-Institut für Astronomie, Universität Bonn, Auf dem Hügel 71, 53121 Bonn, Germany. [23]Herschel Science Centre, European Space Astronomy Centre, European Space Agency (ESA), Post Office Box 78, 28691 Villanueva de la Cañada, Madrid, Spain. [24]School of Physics and Astronomy, University of Nottingham, University Park, Nottingham NG7 2RD, UK. [25]Scottish Universities Physics Alliance, School of Physics and Astronomy, University of St. Andrews, North Haugh, St. Andrews, KY16 9SS, UK. [26]Instituto de Astrofísica de Canarias, C/Vía Láctea s/n, E-38200 La Laguna, Spain. [27]Departamento de Astrofísica, Universidad de La Laguna (ULL), E-38205 La Laguna, Tenerife, Spain. [28]Eureka Scientific, 2452 Delmer Street, Suite 100, Oakland, CA 94602, USA. [29]Goddard Space Flight Center, Code 667, Greenbelt Road, Greenbelt, MD 20771, USA. [30]Astrophysics Group, Physics Department, Blackett Lab, Imperial College London, Prince Consort Road, London SW7 2AZ, UK. [31]Sterrenkundig Observatorium, Universiteit Gent, Krijgslaan 281 S9, B-9000 Gent, Belgium. [32]Department of Physics and Astronomy, University of Louisville, Louisville, KY 40292, USA. [33]Institut d'Astrophysique Spatiale (IAS), Bâtiment 121, F-91405 Orsa, France. [34]Université Paris–Sud 11 and CNRS (UMR 8617), 91400 Orsay, France. [35]Instituto de Fisica de Cantabria, Consejo Superior de Investigaciones Científicas–Universidad de Cantabria, Avenue de Los Castros s/n, Santander 39005, Spain. [36]Astrophysics Research Institute, Liverpool John Moores University Twelve Quays House, Egerton Wharf, Birkenhead CH41 1LD, UK. [37]Astrophysics Branch, NASA Ames Research Center, Mail Stop 245-6, Moffett Field, CA 94035, USA. [38]NASA Goddard Space Flight Center, Code 667, Greenbelt Road, Greenbelt, MD 20771, USA. [39]Department of Astrophysics and The Enrico Fermi Institute, University of Chicago, 5640 South Ellis Avenue, Chicago, IL 60637, USA. [40]Department of Physics and Astronomy, University of Pennsylvania, Philadephia, PA 19104, USA. [41]Rutgers University, Department of Physics and Astronomy, 136 Frelinghuysen Road, Piscataway, NJ 08854–8019, USA. [42]H. H. Wills Physics Laboratory, University of Bristol, Tyndall Avenue, Bristol BS8 1TL, UK. [43]Laboratoire d'Astrophysique de Marseille, UMR6110 CNRS, and Aix-Marseille Université, 38 rue F. Joliot-Curie, F-13388 Marseille, France. [44]School of Mathematical Sciences, Queen Mary, University of London, Mile End Road, London E1 4NS, UK. [45]University of Colorado, Center for Astrophysics and Space Astronomy, 389-UCB, Boulder, CO 80303, USA. [46]Department of Astronomy, University of Maryland, College Park, MD 20742, USA. [47]Observatories of the Carnegie Institution, 813 Santa Barbara Street, Pasadena, CA 91101, USA. [48]Institute for Space and Astronautical Science, Japan Aerospace Exploration Agency, 3-1-1 Yoshinodai, Chuo-ku, Sagamihara 252-5210, Japan. [49]Infrared Processing and Analysis Center, Pasadena, CA 91125, USA. [50]Jeremiah Horrocks Institute, University of Central Lancashire, Preston PR1 2HE, UK. [51]Space Science and Technology Department, Rutherford Appleton Laboratory, Chilton, Didcot, Oxfordshire OX11 0QX, UK. [52]University of British Columbia, 6224 Agricultural Road, Vancouver BC V6T 1Z1, Canada. [53]Institute for Computational Cosmology, Durham University, Durham DH1 3LE, UK. [54]Max-Planck-Institut für Kernphysik (MPIK), Saupfercheckweg 1, 69117 Heidelberg, Germany. [55]Leiden Observatory, Leiden University, Post Office Box 9513, NL-2300 RA Leiden, Netherlands.

*To whom correspondence should be addressed E-mail: m.negrello@open.ac.uk

the number counts (the number of galaxies at a given brightness) of dust-obscured star-forming galaxies, which are usually referred to as submillimeter galaxies (SMGs) (*15*). Because of that, even a small number of highly magnified SMGs can substantially affect the shape of the bright end of the submillimeter source counts enhancing the number of SMGs seen at bright flux densities than would be expected on the basis of our knowledge of the unlensed SMG population (Fig. 1). Furthermore, the frequency of lensing events is relatively high in the submillimeter (*11*) because SMGs are typically at high redshift ($z > \sim 1$) (*16*), and this increases the probability that a SMG is in alignment with, and therefore lensed by, a foreground galaxy. Other important contributors to the bright tail of the submillimeter counts are low-redshift ($z \leq 0.1$) spiral and starburst galaxies (*17*) and higher redshift radio-bright Active Galactic Nuclei (AGNs) (*18*); however, both of these are easily identified, and therefore removed, in relatively shallow optical and radio surveys. Therefore, flux-density–limited submillimeter surveys could provide a sample of lens candidates from which contaminants can be readily removed, leaving a high fraction (close to 100%) of gravitational lens systems (Fig. 1). Because this selection of lens candidates relies only on the properties of the background source (its flux density), it can probe a wide range of lens properties (such as redshifts and masses) and thus provide a valuable sample for studying the elliptical properties of lensing galaxies (*19*) as well as investigating the detailed properties of the lensed SMGs.

The submillimeter lens candidate selection at work. Although the approach presented above may be more efficient and vastly more time-effective than those exploited so far in the radio (*20*) or the optical (*21*, *22*), at least several tens of square degrees (deg^2) of the sky must be observed in the submillimeter to produce a statistically significant sample of strongly lensed objects and a minimal contamination from unlensed galaxies. This is because the surface density of lensed submillimeter galaxies is predicted to be lower than ~0.5 deg^{-2} for flux densities above 100 mJy at 500 μm (Fig. 1). Submillimeter surveys conducted before the advent of Herschel were either limited to small areas of the sky (*15*, *23*) or were severely affected by source confusion due to poor spatial resolution (*24*). Therefore, no previous test of this selection method has been performed, although the SPT has recently mapped an area of more than 80 deg^2 at millimeter wavelengths (*9*) and found an "excess" of sources that could be accounted for by a population of gravitationally lensed objects.

The Herschel Astrophysical Terahertz Large Area Survey (H-ATLAS) (*25*) represents the largest-area submillimeter survey being currently undertaken by Herschel. H-ATLAS uses the Spectral and Photometric Imaging Receiver (SPIRE) (*26*) and the Photodetector Array Camera and Spectrometer (PACS) (*27*, *28*) instruments and, when completed, will cover ~550 deg^2 of the sky from 100 to 500 μm. H-ATLAS has been designed to observe areas of the sky with previously existing multiple-wavelength data: Galaxy Evolution Explorer (GALEX) ultraviolet (UV) data, Sloan Digital Sky Survey (SDSS) optical imaging and spectroscopy, NIR data from the UK Infrared Telescope (UKIRT) Infrared Deep Sky Survey (UKIDSS) Large Area Survey (LAS), spectra from the Galaxy And Mass Assembly (GAMA) (*29*) project, radio-imaging data from the Faint Images of the Radio Sky at Twenty-cm (FIRST) survey and the NRAO Very Large Array Sky Survey (NVSS). The first 14.4 deg^2 of the survey, centered on J2000 RA 09:05:30.0 DEC 00:30:00.0 and covering ~3% of the total area, was observed in November 2009 as part of the Herschel Science Demonstration Phase (SDP). The results were a catalog of ~6600 sources (*30*), with a significance >5σ, in at least one SPIRE waveband, where the noise (σ) includes both instrumental and source confusion noise and corresponds to ~7 to 9 mJy/beam.

The Herschel/SPIRE 500-μm channel is favorable for selecting lens candidates because the submillimeter source counts steepen at longer wavelengths (*24*, *31*). We used theoretical predictions (*14*) to calculate the optimal limiting flux density, above which it is straightforward to remove contaminants from the parent sample and maximize the number of strongly lensed high-redshift galaxies. The surface-density of unlensed SMGs is predicted to reach zero by $S_{500} \sim 100$ mJy (*14*), and these objects are only detectable above this threshold if gravitationally lensed by a foreground galaxy (Fig. 1). The H-ATLAS SDP catalog contains 11 sources with 500 μm flux density above 100 mJy. Ancillary data in the field revealed that six of these objects are contaminants, four are spiral galaxies with spectroscopic redshifts in the range of 0.01 to 0.05 [see (*32*) for a detailed analysis of one of these sources], one is an extended galactic star-forming region, and one is a previously known radio-bright AGN (*33*). Although the number of these sources are few at

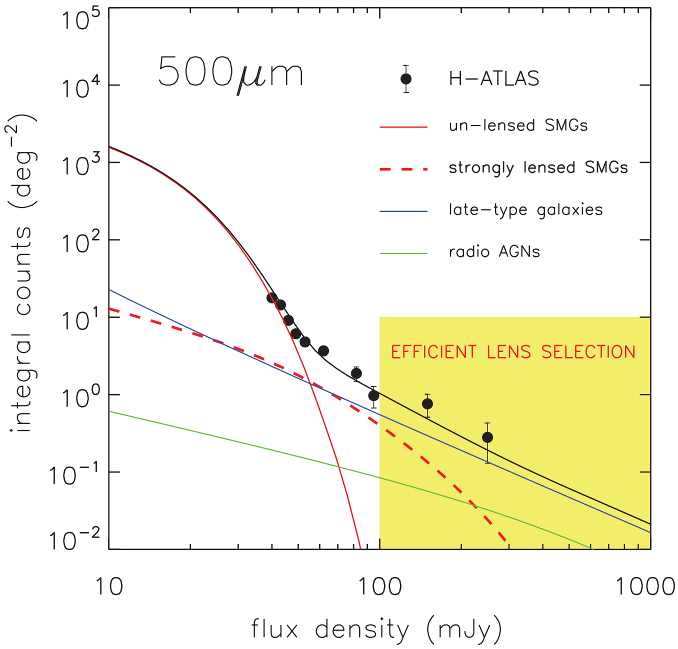

Fig. 1. Selection of gravitational lenses at submillimeter wavelengths. The 500-μm source counts consist of three different populations (*14*): high-redshift SMGs; lower redshift late type (starburst plus normal spiral) galaxies; and radio sources powered by active galactic nuclei. Strongly lensed SMGs dominate over unlensed SMGs at very bright fluxes, where the count of unlensed SMGs falls off dramatically (yellow shaded region). The data points are from H-ATLAS (*31*).

Table 1. Photometric and spectroscopic redshifts of the five lens candidates. Spectroscopic redshifts were derived from optical lines for the lens [$z_{spec}^{(opt)}$] and from CO lines for the background source [$z_{spec}^{(CO)}$]. Photometric redshifts are based on UV/optical/NIR photometry for the lens [$z_{phot}^{(opt)}$] and H-ATLAS plus SMA and MAMBO photometry for the background source [$z_{phot}^{(sub-mm/millimeter)}$; using the photometric redshift code of (*36*, *37*)]. The quoted errors on the redshifts correspond to a 68% confidence interval (CI).

SDP ID	$z_{phot}^{(opt)}$	$z_{spec}^{(opt)}$	$z_{phot}^{(sub-mm/millimeter)}$	$z_{spec}^{(CO)}$
9	0.679 ± 0.057	–	$1.4_{-0.4}^{+0.3}$	1.577 ± 0.008*
11	0.72 ± 0.16	0.7932 ± 0.0012†	$1.9_{-0.3}^{+0.4}$	1.786 ± 0.005*
17	0.77 ± 0.13	0.9435 ± 0.0009†	$2.0_{-0.3}^{+0.4}$	0.942 ± 0.004 and 2.308 ± 0.011*
81	0.334 ± 0.016	0.2999 ± 0.0002‡	$2.9_{-0.3}^{+0.2}$	3.037 ± 0.010* 3.042 ± 0.001§‖
130	0.239 ± 0.021	0.2201 ± 0.002¶	$2.6_{-0.2}^{+0.4}$	2.625 ± 0.001§ 2.6260 ± 0.0003‖

*Datum is from CSO/Z-Spec (*43*). †Datum is from the William Herschel Telescope (*35*). ‡Datum is from SDSS. §Datum is from GBT/Zpectrometer (*45*). ‖Datum is from PdBI (*35*). ¶Datum is from the Apache Point Observatory (*35*).

bright flux densities, the measured surface densities are consistent with expectations (Fig. 1) (*17*, *18*). Exclusion of these contaminants left the five objects that form our sample of lens candidates (table S1) (*35*), identified as ID9, ID11, ID17, ID81, and ID130.

Unveiling the nature of the lens candidates. For gravitational lensing systems selected at submillimeter wavelengths, we would expect the lensing galaxy to be seen in optical and/or NIR images, in which the emission from the lens dominates over the higher redshift background SMG. In line with these expectations, all of the lens candidates have a close counterpart in SDSS or UKIDSS images (or both). A likelihood ratio analysis (*34*) showed that the probability of a random association between these bright submillimeter sources and the close optical/NIR counterparts is less than a few percent. Therefore, the optical and submillimeter emissions must be physically related, either because they occur within the same object or because of the effects of gravitational lensing, boosting the flux of the background source and indirectly affecting the likelihood ratio calculations. The redshift measurements support the later scenario. Although the optical/NIR photometric/spectroscopic redshifts lie in the range of $z \sim 0.3$ to 0.9 (Table 1 and figs. S3 and S4) (*35*), the redshifts estimated from the submillimeter/millimeter spectral energy distributions (SEDs) [following the method described in (*36*, *37*)] are distinctly different (Table 1). The lensed SMG photometric redshifts have been confirmed and made more precise through the spectroscopic detection, in these objects, of carbon monoxide (CO) rotational line emission, which are tracers of molecular gas associated to star-forming environments. Until recently, these kinds of detections were difficult to achieve without prior knowledge of the source redshift, which required extensive optical/NIR/radio follow-up observations. Because of the development of wide-bandwidth radio spectrometers capable of detecting CO lines over a wide range of redshifts, it is now possible for blind redshift measurements of SMGs to be taken without relying on optical or NIR spectroscopy (*38*, *39*). ID81 was observed with the Z-Spec spectrometer (*40*, *41*) on the California Institute of Technology Submillimeter Observatory. The data revealed several CO lines redshifted into the frequency range of 187 to 310 GHz; the strongest of these lines has been interpreted as the CO J=7–6 line, with an estimated redshift of $z = 3.04$ (*42*). This represents the first blind redshift determination by means of Z-Spec. We followed up this observation with the PdBI and detected CO J=3–2 and CO J=5–4 emission lines, redshifted to $z = 3.042$, confirming the Z-Spec–measured redshift (*35*). We also used the Zpectrometer instrument (*43*, *44*) on the NRAO Robert C. Byrd Green Bank Telescope (GBT) to obtain an independent confirmation of the redshift of ID81 (Table 1 and fig. S1) (*35*, *45*) and to measure the redshift of ID130. We detected redshifted CO J=1–0 emission at $z = 2.625$ in the spectrum of ID130 (fig. S1) (*35*, *45*). This redshift was confirmed by the PdBI with the observation of CO J=3–2 and CO J=5–4 lines, yielding a redshift of $z = 2.626$ (*35*). The Z-Spec spectrometer

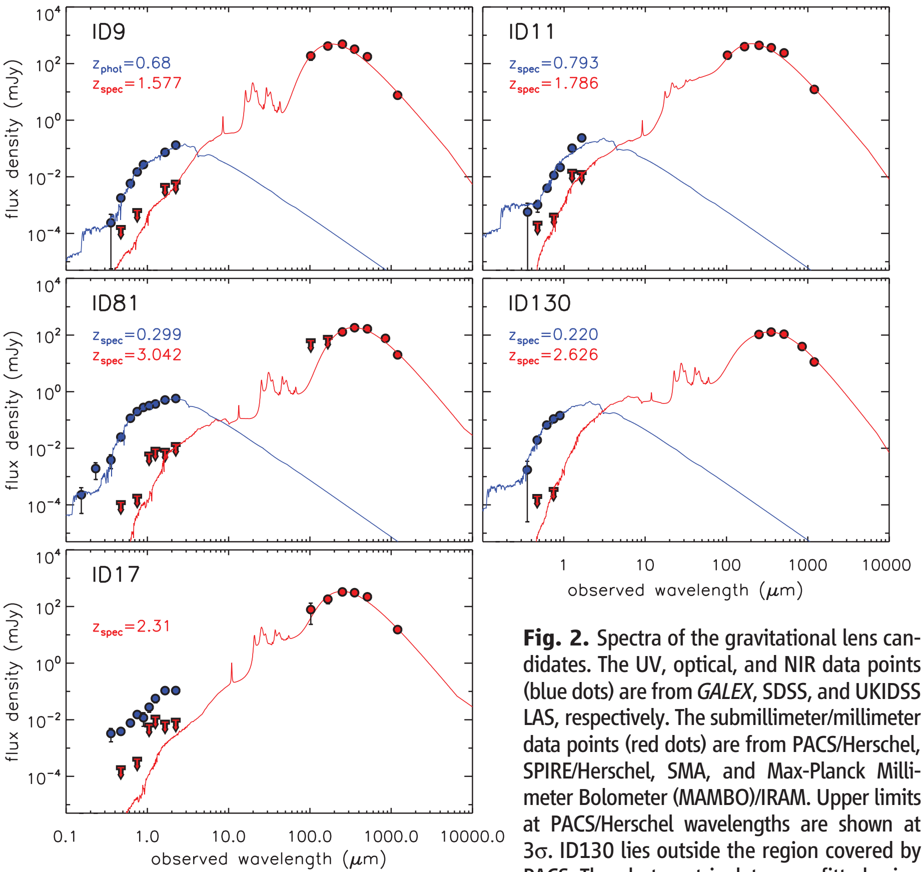

Fig. 2. Spectra of the gravitational lens candidates. The UV, optical, and NIR data points (blue dots) are from *GALEX*, SDSS, and UKIDSS LAS, respectively. The submillimeter/millimeter data points (red dots) are from PACS/Herschel, SPIRE/Herschel, SMA, and Max-Planck Millimeter Bolometer (MAMBO)/IRAM. Upper limits at PACS/Herschel wavelengths are shown at 3σ. ID130 lies outside the region covered by PACS. The photometric data were fitted using SED models from (*47*). The background source, responsible for the submillimeter emission, is a heavily dust-obscured star-forming galaxy (red solid curve), whereas the lens galaxy, which is responsible for the UV/optical and NIR part of the spectrum, is characterized by passive stellar evolution.

Table 2. Derived parameters for the five lens candidates. Estimated mass in stars (M_*) and Star Formation Rate (SFR) of the foreground galaxy derived from the best-fit to the UV/optical/NIR part of the SED; the Einstein radius measured from the SMA images (θ_E); mass within the Einstein radius (M_E) estimated from θ_E; line-of-sight stellar velocity dispersion ($\sigma^{FJ}{}_v$) derived from the Faber-Jackson relation and the B-band luminosity produced by the best-fit to the UV/optical/NIR SED; Einstein radius ($\theta^{FJ}{}_E$) calculated from $\sigma^{FJ}{}_v$; infrared luminosity of the background source (L_{IR}), without correction for magnification, derived by fitting the submillimeter/millimeter part of the SED and the upper limits at optical and NIR wavelengths (Fig. 2); and visual extinction parameter (A_V) inferred for the background galaxy. All the quoted errors correspond to a 68% CI. For ID17, only the infrared luminosity and the extinction parameter of the background source are quoted because the lensing mass probably consists of two galaxies that can only be disentangled in the Keck images. The symbols $M_\odot$ and $L_\odot$ denote the total mass and the total luminosity of the Sun, respectively, and correspond to $M_\odot = 1.99 \times 10^{30}$ kg and $L_\odot = 3.839 \times 10^{33}$ erg s^{-1}. Dashes indicate lack of constraint.

SDP ID	log(M_*) ($M_\odot$)	log(SFR) ($M_\odot$ yr^{-1})	θ_E (arc sec)	log(M_E) ($M_\odot$)	$\sigma^{FJ}{}_v$ (km sec^{-1})	$\theta^{FJ}{}_E$ (arc sec)	log(L_{IR}) ($L_\odot$)	A_V
9	$10.79_{-0.11}^{+0.16}$	$-0.51_{-0.27}^{+0.20}$	—	—	232_{-56}^{+75}	$0.77_{-0.34}^{+0.49}$	$13.48_{-0.06}^{+0.07}$	$6.7_{-1.0}^{+1.5}$
11	$11.15_{-0.10}^{+0.09}$	$-0.08_{-0.24}^{+0.18}$	—	—	258_{-62}^{+82}	$0.91_{-0.40}^{+0.59}$	$13.61_{-0.06}^{+0.06}$	$5.1_{-0.7}^{+1.6}$
17	—	—	—	—	—	—	$13.57_{-0.06}^{+0.08}$	$5.3_{-0.6}^{+1.4}$
81	$11.17_{-0.08}^{+0.04}$	$-1.66_{-0.14}^{+0.46}$	1.62 ± 0.02	11.56 ± 0.01	242_{-58}^{+77}	$1.51_{-0.67}^{+0.98}$	$13.71_{-0.07}^{+0.07}$	$3.5_{-0.3}^{+3.4}$
130	$10.65_{-0.08}^{+0.06}$	$-1.17_{-0.58}^{+0.39}$	0.59 ± 0.02	10.57 ± 0.04	174_{-42}^{+55}	$0.81_{-0.36}^{+0.52}$	$13.45_{-0.09}^{+0.08}$	$1.9_{-0.3}^{+0.3}$

observed the remaining three lens candidates (*42*) and detected CO lines at redshifts of $z = 1.577$ and $z = 1.786$ for ID9 (fig. S2) (*35*) and ID11, respectively, which are higher and inconsistent with the redshifts derived from the optical photometry/spectroscopy (Table 1). The Z-Spec CO measurements for ID17 are indicative of two redshifts; one, $z = 0.942$, that is in agreement with the optical redshift and a higher one, $z = 2.31$, which is indicative of a more distant galaxy.

To determine the morphological type of the foreground galaxies, we obtained high-resolution optical images for all five objects with the Keck telescope at *g*- and *i*-bands (*35*). ID9, ID11, ID81, and ID130 all have optical profiles that are consistent with elliptical galaxies (figs. S5 and S6 and table S4) (*35*). The interpretation of the results for ID17 is complicated by the presence of two partially superimposed galaxies in the optical images (fig. S7) (*35*), neither exhibiting the disturbed morphology expected for lensed objects. This indicates that ID17 may be a gravitational lens system with two foreground lensing masses at similar redshifts ($z \sim 0.8$ to 0.9)—possibly a merging system—with some molecular gas responsible for the CO emission detected by Z-Spec at $z \sim 0.9$ and confirmed with optical spectroscopy (Table 1). A fit to the UV/optical/NIR SEDs of ID9, ID11, ID81, and ID130 (*46*), using the models of (*49*), gives stellar masses in the range of 4×10^{10} to 15×10^{10} $M_\odot$ (Table 2) and almost negligible present-day star formation, which is consistent with elliptical galaxies (Fig. 2).

For all five lens systems, the background source appears to be undetected in the Keck *g*- and *i*-band images, despite the flux magnification due to lensing. After subtracting the best-fit light profile from each lens (figs. S5 to S7) (*36*), we found no structure that could be associated with the background source in the residual images (figs. S5 and S6). We derived 3-σ upper limits from the residual maps (table S3) and corresponding NIR limits from the UKIDSS images. These upper limits were used to fit the SEDs of the background sources assuming the models of (*47*), calibrated to reproduce the UV-to-infrared SEDs of local, purely star-forming ultraluminous infrared galaxies (ULIRG) ($10^{12} \leq L_{IR}/L_\odot < 10^{13}$) (*48*). A visual extinction (*49*) of $A_V > 2$ is required to be consistent with the optical/NIR upper limits (Fig. 2 and Table 2), confirming severe dust obscuration in these galaxies along the line of sight. Our results indicate that these submillimeter bright gravitationally lensed galaxies would have been entirely missed by standard optical methods of selection.

We obtained observations at the SMA for ID81 and ID130 at 880 μm, with the aim of detecting the lensed morphology of the background galaxy (*35*). The SMA images reveal extended submillimeter emission distributed around the cores of the foreground elliptical galaxies, with multiple peaks (four main peaks in ID81 and two in ID130), which is consistent with a lensing interpretation of these structures (Fig. 3). The position of these peaks can be used to directly constrain the Einstein radius—the radius of the circular region on the sky (the Einstein ring) into which an extended source would be lensed if a foreground galaxy were exactly along the line of sight of the observer to the source (for a perfectly circular lens). The Einstein radius is a measure of the projected mass of the lens, so it can be used to derive the total (dark plus luminous) mass of the galaxy within the Einstein radius (Table 2) (*35*). Another measure of the total mass of a lens is the line-of-sight stellar velocity dispersion, σ_v. We have estimated σ_v from the local Faber–Jackson (FJ) relation (*50*) between σ_v and the rest-frame B-band luminosity for elliptical galaxies. Assuming passive stellar evolution for the lens galaxies, which is appropriate for elliptical galaxies, we have extrapolated their rest-frame K-band luminosity to $z = 0$ [using the evolutionary tracks of

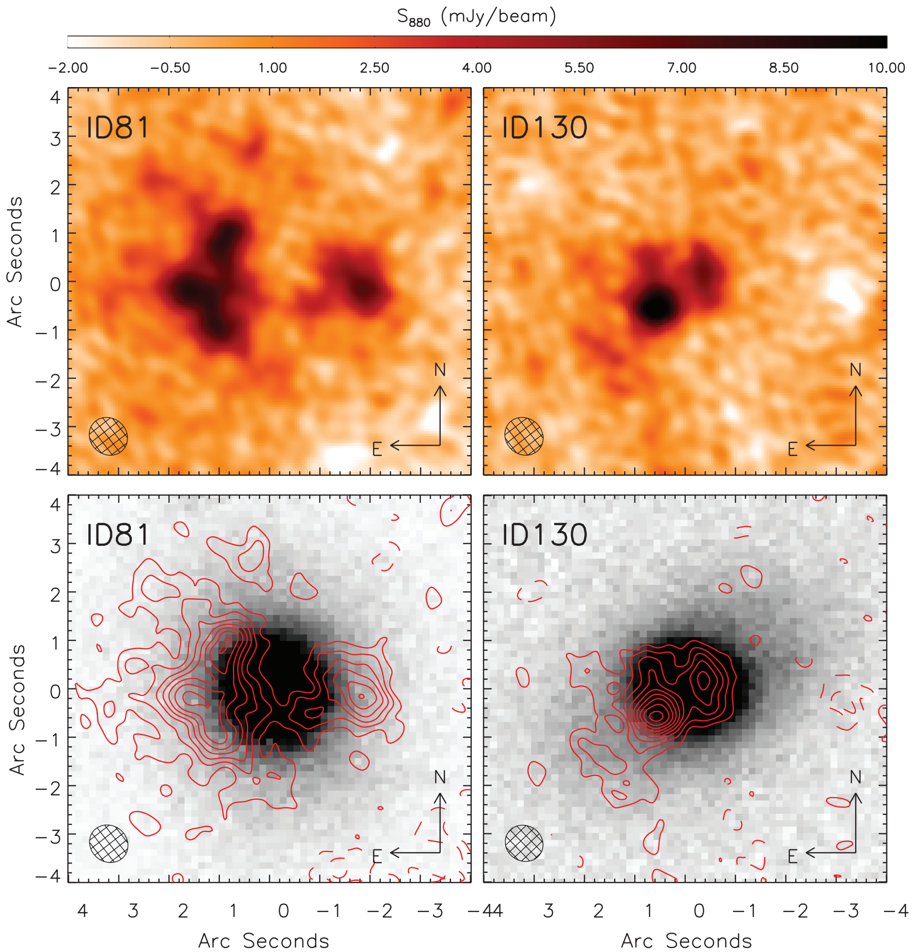

Fig. 3. Submillimeter and optical follow-up imaging of ID81 and ID130. The SMA images of ID81 and ID130 are shown in the top panels, centered on the optical counterpart, and were obtained by combining the visibility data from very extended, compact, and subcompact configuration observations. The Keck i-band image of ID81 and ID130 are shown in the bottom panels with the SMA contours superimposed (in red). The contours are in steps of −2σ, 2σ, 4σ, 6σ, 8σ, 10σ…, with σ = 0.6 mJy/beam. The SMA synthesized beam is shown in the bottom-left corner.

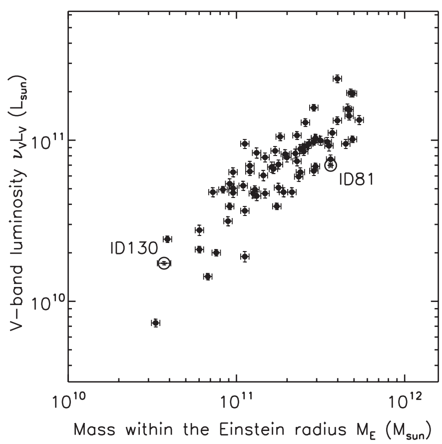

Fig. 4. Relationship between mass and luminosity for the lensing galaxy in ID81 and ID130. The rest-frame *V*–band luminosity was derived from the best-fit SED to the UV/optical/NIR photometric data; the mass within the Einstein radius is that measured directly from the SMA images. The light versus mass relation inferred for ID81 and ID130 (open circles) is consistent with that observed for the SLACS lenses [black dots, from (*54*), assuming an uncertainty of 0.025 dex in their mass estimates].

(51)] and then converted this to B-band luminosity using the B – K = 4.43 color relation from (52). The result was then applied to the FJ relation from (53). Given a mass model for the lens (35), we can predict the Einstein radius of the galaxy from the value of σ_v expected from the FJ relation and compare it with that directly measured from the SMA images (Table 2). Although the value of the Einstein radius derived from the line-of-sight stellar velocity dispersion is affected by large uncertainties (as a result of the scatter in the FJ relation), it is consistent with the value measured in the SMA images for both ID81 and ID130. In order to test whether the properties of the lensing galaxies in our sample are consistent with those of other known lens ellipticals at similar redshift, we compared the V-band mass-to-light ratio of the lens galaxy for ID81 and ID130 with those measured in the Sloan Lens Advanced Camera for Surveys (ACS) Survey (SLACS) (Fig. 4) (54), which cover a similar redshift range ($z \sim 0.1$ to 0.3). The agreement with the average trend revealed by SLACS confirms that our lens selection method is not biased to lensing ellipticals with atypical luminosities. Moreover, the location of ID130 in Fig. 4 indicates that our selection method can probe lower masses and lower luminosity lens galaxies than those sampled by SLACS, thus offering a wider range in lens properties to be investigated.

The best-fit SED to the submillimeter/millimeter photometry for each of the five background sources give infrared luminosities $L_{IR} \geq \sim 3 \times 10^{13} L_{\odot}$ (Table 2), which would classify these objects as Hyper Luminous Infra-Red galaxies (HLIRGs) ($L_{IR} \geq 10^{13} L_{\odot}$). However, a correction for magnification because of lensing will reduce these values by a factor of 10 or greater. For example, assuming that the light distribution of the background source is described by a Gaussian profile with a full width at half maximum (FWHM) of 0.2 arcseconds [which is consistent with the physical extension of the background galaxy in (4)], the best-fit lens model (fig. S9) (35) predicts total amplifications of ~19 and ~6 for ID81 and ID130, respectively. Typical amplifications of 8 to 10 are also suggested by (14); therefore, it is more likely that these sources are ULIRGs.

These results already provide constraints for models of the formation and evolution of massive galaxies at high redshift. The fact that many (if not all) of the brightest SMGs detected in the H-ATLAS SDP field are amplified by lensing implies that unlensed $z > 1$ star-forming galaxies with flux densities of more than 100 mJy at 500 μm are rare, with ≤4.6 of them per 14.4 deg^{-2}, at 99% probability (assuming Poisson statistics). This translates into a 0.32 deg^{-2} upper limit on the surface density of these sources. The same limit should translate to the abundance of HLIRGs with $L_{IR} > 5 \times 10^{13} L_{\odot}$ at $z < 4$ because they would also have 500-μm flux densities above 100 mJy, which has possible implications for the role of feedback during the formation of the most massive galaxies in the universe. By extrapolating our SDP findings to the full H-ATLAS field, we predict a total sample of more than 100 bright-lensed sources, with which we can further improve this constraint.

References and Notes

1. When multiple images of the same background source are formed, the event is known as strong gravitational lensing.
2. P. J. Marshall *et al.*, *Astrophys. J.* **671**, 1196 (2007).
3. D. P. Stark *et al.*, *Nature* **455**, 775 (2008).
4. A. M. Swinbank *et al.*, *Nature* **464**, 733 (2010).
5. I. Smail, R. J. Ivison, A. W. Blain, *Astrophys. J.* **490**, L5 (1997).
6. A. W. Blain, J. Kneib, R. J. Ivison, I. Smail, *Astrophys. J.* **512**, L87 (1999).
7. M. Rowan-Robinson *et al.*, *Nature* **351**, 719 (1991).
8. I. Smail, R. J. Ivison, A. W. Blain, J. Kneib, *Mon. Not. R. Astron. Soc.* **331**, 495 (2002).
9. J. D. Vieira *et al.*, *Astrophys. J.* **719**, 763 (2010).
10. G. L. Pilbratt *et al., Atron. Astrophys.* **518**, L1 (2010) (10.1051/0004-6361/201014759).
11. A. W. Blain, *Mon. Not. R. Astron. Soc.* **283**, 1340 (1996).
12. F. Perrotta, C. Baccigalupi, M. Bartelmann, G. De Zotti, G. L. Granato, *Mon. Not. R. Astron. Soc.* **329**, 445 (2002).
13. F. Perrotta *et al.*, *Mon. Not. R. Astron. Soc.* **338**, 623 (2003).
14. M. Negrello *et al.*, *Mon. Not. R. Astron. Soc.* **377**, 1557 (2007).
15. K. Coppin *et al.*, *Mon. Not. R. Astron. Soc.* **372**, 1621 (2006).
16. S. C. Chapman, A. W. Blain, I. Smail, R. J. Ivison, *Astrophys. J.* **622**, 772 (2005).
17. S. Serjeant, D. Harrison, *Mon. Not. R. Astron. Soc.* **356**, 192 (2005).
18. G. de Zotti *et al.*, *Astron. Astrophys.* **431**, 893 (2005).
19. L. V. E. Koopmans, T. Treu, A. S. Bolton, S. Burles, L. A. Moustakas, *Astrophys. J.* **649**, 599 (2006).
20. I. W. A. Browne, The Class Collaboration, *Astron. Soc. Pac. Conf. Ser.* **237**, 15 (2001).
21. M. Oguri *et al.*, *Astron. J.* **132**, 999 (2006).
22. C. Faure *et al.*, *Astrophys. J.* **176**, 19 (2008).
23. A. Weiß *et al.*, *Astrophys. J.* **707**, 1201 (2009).
24. M. J. Devlin *et al.*, *Nature* **458**, 737 (2009).
25. S. Eales *et al.*, *Publ. Astron. Soc. Pac.* **122**, 499 (2010).
26. M. J. Griffin *et al.*, *Astron. Astrophys.* **518**, L3 (2010).
27. A. Poglitsch *et al.*, *Astron. Astrophys.* **518**, L2 (2010).
28. E. Ibar *et al.*, *Astrophys. J.*, in press; preprint available at http://xxx.lanl.gov/abs/astro-ph/1009.0262.
29. S. Driver *et al.*, *Astrophys. J.*, in press; preprint available at http://xxx.lanl.gov/abs/astro-ph/1009.0614.
30. S. J. Maddox *et al.*, *Astron. Astrophys.* **518**, L11 (2010).
31. D. L. Clements *et al.*, *Astron. Astrophys.* **518**, L8 (2010).
32. M. Baes *et al.*, *Astron. Astrophys.* **518**, L39 (2010).
33. J. González-Nuevo *et al.*, *Astron. Astrophys.* **518**,L38 (2010).
34. D. J. B. Smith *et al.*, *MNRAS*, in press; preprint available at http://arxiv.org/abs/1007.5260.
35. Supporting online material (SOM) text is available on *Science* Online.
36. D. H. Hughes *et al.*, *Mon. Not. R. Astron. Soc.* **335**, 871 (2002).
37. I. Aretxaga *et al.*, *Mon. Not. R. Astron. Soc.* **342**, 759 (2003).
38. A. Weiß *et al.*, *Astrophys. J.* **705**, L45 (2009).
39. E. Daddi *et al.*, *Astrophys. J.* **695**, L176 (2009).
40. B. J. Naylor *et al.*, *Soc. Photo-Opt. Instrum. Eng. (SPIE) Conf. Ser.* **4855**, 239 (2003).
41. C. M. Bradford *et al.*, *Astrophys. J.* **705**, 112 (2009).
42. R. Lupu, submitted (available at http://xxx.lanl.gov/abs/astro-ph/1009.5983) (2010).
43. A. I. Harris *et al.*, *Astron. Soc. Pac. Conf. Ser.* **375**, 82 (2007).
44. The Zpectrometer frequency coverage allows it to search for CO J=1–0 transition over the redshift range of 2.2 to 3.5 simultaneously.
45. D. Frayer *et al.*, *Astrophys. J.*, in press; preprint available at http://xxx.lanl.gov/abs/astro-ph/1009.2194.
46. Only g- and i-band photometry can be obtained for each of the two galaxies detected in ID17. For this reason, we did not attempt any fit to the optical/NIR SED of this H-ATLAS source.
47. E. da Cunha, S. Charlot, D. Elbaz, *Mon. Not. R. Astron. Soc.* **388**, 1595 (2008).
48. E. da Cunha *et al.*, *Astrophys. J.*, in press; preprint available at http://xxx.lanl.gov/abs/astro-ph/1008.2000.
49. The visual extinction parameter, A_V, is the difference between the observed V-band magnitude and the intrinsic (dust-free) V-band magnitude of the galaxy.
50. S. M. Faber, R. E. Jackson, *Astrophys. J.* **204**, 668 (1976).
51. C. J. Willott, S. Rawlings, M. J. Jarvis, K. M. Blundell, *Mon. Not. R. Astron. Soc.* **339**, 173 (2003).
52. J. Huang, L. L. Cowie, G. A. Luppino, *Astrophys. J.* **496**, 31 (1998).
53. D. H. Gudehus, *Astrophys. J.* **382**, 1 (1991).
54. M. W. Auger *et al.*, *Astrophys. J.* **705**, 1099 (2009).

55. Herschel is an ESA space observatory with science instruments provided by European-led principal investigator consortia and with important participation from NASA. U.S. participants in H-ATLAS acknowledge support from NASA through a contract from JPL. This work was supported by the Science and Technology Facilities Council (grants PP/D002400/1 and ST/G002533/1) and studentship SF/F005288/1. We thank Agenzia Spaziale Italiana (ASI) for funding through contract No. I/016/07/0 COFIS and ASI/Istituto Nazionale di Astrofisica agreement I/072/09/0 for the Planck Low-Frequency Instrument (LFI) Activity of Phase E2. Research supported in part by Consejo Nacional de Ciencia y Tecnología (CONACyT) grants 39953-F and 39548-F. The W. M. Keck Observatory is operated as a scientific partnership among the California Institute of Technology, the University of California, and NASA. The Observatory was made possible by the generous financial support of the W. M. Keck Foundation. The Submillimeter Array is a joint project between the Smithsonian Astrophysical Observatory and the Academia Sinica Institute of Astronomy and Astrophysics and is funded by the Smithsonian Institution and the Academia Sinica. IRAM is supported by Institut National des Sciences de l'Univers (INSU)/CNRS (France), Max Planck Society (MPG) (Germany), and Instituto Geográfico Nacional (IGN) (Spain). Z-spec was supported by NSF grant AST-0807990 to J.A. and by the CSO NSF Cooperative Agreement AST-0838261. Support was provided to J.K. by an NSF Graduate Research Fellowship. Z-spec was constructed under NASA SARA grants NAGS-11911 and NAGS-12788 and an NSF Career grant (AST-0239270) and a Research Corporation Award (RI0928) to J.G., in collaboration with JPL, California Institute of Technology, under a contract with NASA. Construction of and observations with the Zpectrometer have been supported by NSF grants AST-0503946 and AST-0708653. NRAO is a facility of the NSF operated under cooperative agreement by Associated Universities. The optical spectroscopic redshift of ID130 was derived from observations obtained with the Apache Point Observatory 3.5-m telescope, which is owned and operated by the Astrophysical Research Consortium. The optical spectroscopic redshifts of ID9 and ID11 were obtained with the William Herschel Telescope, which is operated on the island of La Palma by the Isaac Newton Group in the Spanish Observatorio del Roque de los Muchachos of the Instituto de Astrofísica de Canarias. For the use of Keck, SMA, and CSO, the authors wish to recognize and acknowledge the very important cultural role and reverence that the summit of Mauna Kea has always had within the indigenous Hawaiian community. We are most fortunate to have the opportunity to conduct observations from this mountain.

Supporting Online Material

www.sciencemag.org/cgi/content/full/330/6005/800/DC1
SOM Text
Figs. S1 to S9
Tables S1 to S4
References

8 June 2010; accepted 21 September 2010
10.1126/science.1193420